PHYSICAL REVIEW E **89**, 050701(R) (2014)

# Dynamic force patterns of an undulatory microswimmer

Rafael D. Schulman,[1] Matilda Backholm,[1] William S. Ryu,[2] and Kari Dalnoki-Veress[1,3,*]

[1]*Department of Physics and Astronomy and The Brockhouse Institute for Materials Research, McMaster University, 1280 Main Street West, Hamilton, Ontario, Canada L8S 4M1*

[2]*Department of Physics, University of Toronto, 60 St. George Street, Toronto, Ontario, Canada M5S 1A7*

[3]*Laboratoire de Physico-Chimie Théorique, UMR CNRS Gulliver 7083, ESPCI, Paris, France*

(Received 23 January 2014; published 30 May 2014)

We probe the viscous forces involved in the undulatory swimming of the model organism *C. elegans*. Using micropipette deflection, we attain direct measurements of lateral and propulsive forces produced in response to the motion of the worm. We observe excellent agreement of the results with resistive force theory, through which we determine the drag coefficients of this organism. The drag coefficients are in accordance with theoretical predictions. Using a simple scaling argument, we obtain a relationship between the size of the worm and the forces that we measure, which well describes our data.

DOI: 10.1103/PhysRevE.89.050701 PACS number(s): 87.19.ru, 47.63.Gd, 47.15.G−

Locomotion through a fluid environment is common to organisms over a wide range of length scales, from whales and humans to primitive algae and bacteria. However, the physics of "microswimming," which is the propulsion at very small length scales, differs vastly from that applicable to macroscopic swimmers. Studying the principles of locomotion in this regime is crucial for our fundamental understanding of a diverse collection of organisms, including bacteria, sperm, and a variety of other microorganisms. Furthermore, microswimmers offer a wide variety of applications including robotic microswimmers capable of cargo towing for biomedical purposes, such as advanced drug targeting [1,2], collective swimming of bacteria to induce mixing in microfluidic devices [3,4], and fluid pumping [5–7].

The Reynolds number is a quantity that measures the relative magnitude of viscous and inertial forces in a fluid. At small length scales, the Reynolds number is typically less than unity, which implies that viscous forces are dominant and inertia can be neglected. In addition, to achieve propulsion in this regime, it is obligatory to perform a motion that is not time reversible, according to the scallop theorem [8]. This theorem asserts that if a swimmer performs a sequence of motions that is unchanged when played in reverse, such as a scallop, which simply opens and closes, it will not acquire any net displacement. There are numerous ways of breaking this symmetry, such as the helical beating of a flagellum [8–10], and motions similar to a human breast stroke, as is performed by the simple alga cell *Chlamydomonas reinhardtii* [11,12]. Another common way to break this symmetry is to propagate traveling waves down a body, which is successfully achieved by undulatory swimmers [13–16].

Undulatory locomotion is known to be a very efficient mechanism of propulsion and is effective over a large range of length scales [17]. Extensive theoretical efforts have been put forth in understanding the locomotion of a slender undulator, in which the length of the swimmer is much larger than its width [10,15,16,18,19]. Among these, resistive force theory (RFT) is a simple model in which the viscous force on a body segment moving through a low Reynolds number fluid can be decomposed into a component tangential and normal to that segment [10,15,16,18,20]. Each of these components is linearly proportional to the speed of the segment in that direction and related through the normal and tangential drag coefficients, $c_N$ and $c_T$. The ratio $c_N/c_T$ has important implications in the propulsion of the swimmer. Namely, if $c_N/c_T > 1$, propulsion is directed contrary to the direction of the traveling wave. If $c_N/c_T < 1$, we are faced with the curious case of the undulator moving in the same direction as its traveling wave, while the swimmer can attain no net propulsion if $c_N/c_T = 1$. In RFT, the difficulty lies in determining the drag coefficients. Several theoretical studies have derived

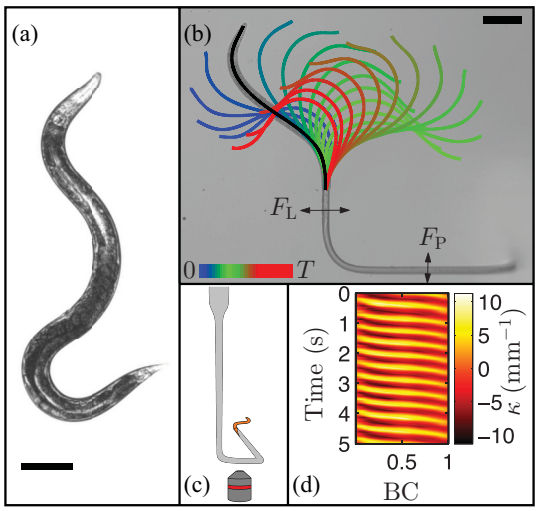


FIG. 1. (Color online) (a) *C. elegans*. The scale bar represents 100 $\mu$m. (b) Time lapse of the worm's centerline over one period ($T$), with colors representing time. A sample centerline is overlaid on the worm in black. Arrows indicate motion of the end of the pipette as a result of the two orthogonal forces. The scale bar represents 150 $\mu$m. (c) Schematic of the micropipette used in our experiments with a worm held at the end (not to scale). (d) Curvature color plot for the swimming. BC (body coordinate) denotes the distance along the worm, where 0 represents the head and 1 represents the portion of the worm nearest the pipette. Positive curvatures are indicated by lighter color and denote the convex side to the left.

*dalnoki@mcmaster.ca

 

values for the coefficients; however, assumptions regarding the swimming and approximations must be made [10,15,18,20]. Indeed, experimental measurements are crucial in order to evaluate the validity of RFT and to determine the magnitude of the drag coefficients. There have been experiments which have evaluated RFT for a variety of single-celled organisms using kinematic data from high-speed imaging [21–23]. Other experiments have performed average force measurements of nonundulatory microorganisms in optical traps [24,25]. However, to date, direct and time-resolved measurements of drag forces on an undulating microswimmer are still lacking. Furthermore, direct verification of the applicability of RFT for swimmers at length scales where the Reynolds number may not be much less than unity is still needed.

Many experiments on undulatory microswimmers have focused on the model organism *Caenorhabditis elegans* [Fig. 1(a)], a millimeter sized hermaphroditic nematode [26]. These studies have characterized the kinematics of *C. elegans* in various environments, including swimming in a buffer of various viscosities [27,28], viscoelastic media [29], crawling on agar [30], structured environments [31,32], and through complex environments such as granular materials [33,34]. Attempts have been made to measure crawling forces using pillars as force transducers for *C. elegans* crawling on agar [35,36]. In another work, the viscous forces of swimming *C. elegans* were inferred from particle tracking and particle image velocimetry [28]. However, these studies, though insightful, have not succeeded in performing direct measurements of forces and drag coefficients in fluid.

Here we present a method to directly measure the time-varying propulsive and lateral forces of *C. elegans*. A comparison between our experimentally determined forces and the calculated forces from RFT demonstrates an excellent agreement. The experimental and theoretical force curves are used to deduce values for the drag coefficients of *C. elegans* swimming. Finally, a simple scaling argument is presented which postulates a relationship between the size of the worm and the mean propulsive and rms lateral force. We find our experimental data to be well described by the scaling argument.

We use a micropipette deflection technique to measure the forces generated by the undulatory microswimmer [37–39]. In this technique, a flexible glass micropipette that is more than three orders of magnitude thinner than its length deflects when subjected to an external force. Since the bending stiffness of the pipette has been determined through calibration, forces can be computed from deflections of the pipette. We catch worms by their tail end by applying suction, and hold them with the end of our pipettes. The micropipettes are capable of deflecting along the worm's swimming axis, as well as along the corresponding in-plane perpendicular direction. Thus, we can measure forces in two orthogonal directions [Figs. 1(b) and 1(c)] [39]. As the nematodes move, they generate forces in their propulsive and lateral directions, which we independently measure using the micropipette as a force transducer [Fig. 1(c)]. The deflections of the pipette are much smaller than length scales associated with the motion of the worms [39].

Upon capture, the worms perform a highly reproducible and periodic sequence of body movements, in which traveling waves are propagated down the body, which is akin to free swimming of *C. elegans* [Fig. 1(b)] [27,28]. However, when held fixed at one end, the traveling waves are of larger amplitude than in free swimming and have a node at the fixed end. The temporal oscillations of the curvature of the worm exhibit a well defined frequency, which remains constant at $2.4 \pm 0.2$ Hz for worms of various lengths [Fig. 1(d)]. The spatial and temporal oscillations in the curvature compare well with what has been measured for free swimming [27,28,31].

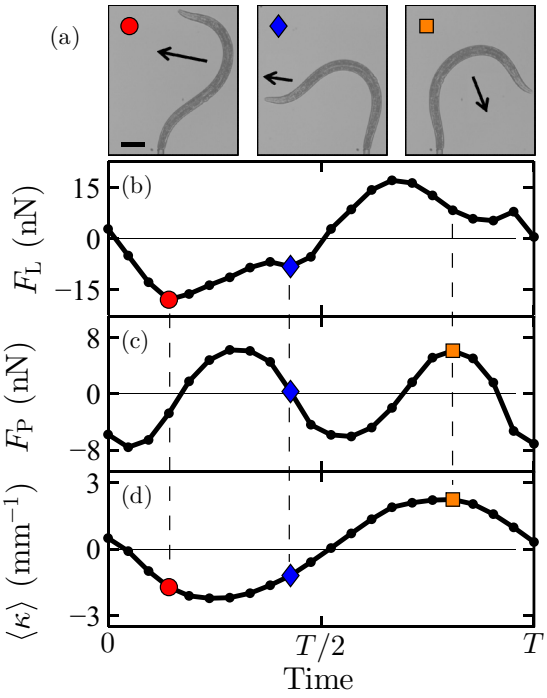


FIG. 2. (Color online) (a) Snapshots of a young adult worm at different stages of one swimming cycle. The labels refer to the markers in the graphs below and the arrows indicate the main velocity of the body. The scale bar represents 100 $\mu$m. (b) The lateral force experienced by the worm over one period, where a positive force denotes a force directed to the left. The peak negative force (red circle) corresponds to the worm moving directly left, generating a drag force to the right (negative direction). Secondary peaks (blue diamond) correspond to turning points in the swimming cycle, when an extra push in the lateral direction is instigated. This point roughly coincides with a zero in the propulsive force. (c) The propulsive force on the worm over one period, where a positive force denotes a force directed up (in the swimming direction). The maximum propulsive force (orange square) corresponds to the worm pushing fluid behind itself, generating a drag force forward. This point roughly coincides with a maximum in the curvature. (d) The mean curvature of the worm over one period.

Figure 2 shows direct *simultaneous measurements* of the force generated in the lateral and propulsive directions as well as images of the motion that caused specific forces [39]. Microswimmers inhabit a low Reynolds number environment, and as such, the net forces involved in swimming are dominated by viscous drag forces. The estimated Reynolds numbers for the worms in these experiment lie within the range 0.05–0.5 [39]. Thus, we are in a regime where inertial effects may not be negligible. However, it is known from previous work that *C. elegans* swimming in a buffer can indeed be treated as a

low Reynolds number swimmer, which suggests that viscous effects may dominate in our system [28]. Using this reasoning, the peak lateral forces ($F_L$) occur when the worm is moving with the greatest speed in the lateral direction [Fig. 2(b)]. Conversely, the largest propulsive forces ($F_P$) are generated when the worms push the greatest amount of fluid behind themselves [Fig. 2(c)]. Small secondary peaks can be found in the lateral force curve corresponding to turning points in the worm's cycle, in which the lateral motion experiences a small spike, and there is minimal motion in the propulsive direction. The maximum propulsive forces approximately coincide with the points of highest mean worm curvature $\langle\kappa\rangle$ [Fig. 2(d)].

In the low Reynolds number regime, drag forces are simply linearly proportional to velocities. According to RFT, one can deconstruct the drag force ($dF$) acting on each length segment ($dl$) of a slender body into forces in two orthogonal directions,

$$dF_T = -c_T v_T \mu\, dl, \quad dF_N = -c_N v_N \mu\, dl, \tag{1}$$

where $\mu$ and $v$ denote the dynamic viscosity and speed respectively, $c$ is the drag coefficient per unit length, and T and N denote directions tangential and normal to the length segment [15]. Since a slender body has little variation in thickness, $c_N$ and $c_T$ can be approximated as constants over the entire length of the swimmer. Although an experimental measurement of these two drag coefficients individually for this microscopic undulator is still needed, the ratio $c_N/c_T$ has been determined through theory and experiment to be approximately 1.5 for body and swimming parameters characteristic of *C. elegans* [10,16,28]. If $c_N$ and $c_T$ are known, using this prescription, and given the speed of each segment of the undulator's body, it is possible to calculate the total drag force the swimmer experiences. Since our experiment is performed in conjunction with high-speed imaging, we can extract the velocities of the worm body. Using numerical integration, we generate the RFT prediction for the lateral and propulsive force curves. Subsequently, using two free parameters, we fit the RFT prediction of the two force curves to our lateral and propulsive data (Fig. 3). In our analysis, we fix $c_N/c_T$ at 1.5 because our fits are not sensitive enough given the experimental error in the data to accurately determine this ratio. Thus, the first free parameter in our fitting controls the magnitude of the two drag coefficients, and functions as a vertical stretch on the curves. We find these drag coefficients to vary little for worms of all sizes ranging from ∼400 to ∼1200 $\mu$m (this agrees with the theoretical prediction of a weak logarithmic dependence on geometry, in which there is no dependence if the swimmer is self-similar for all sizes [10,15,18]), and measure $c_N = 5.1 \pm 0.3$, and $c_T = 3.4 \pm 0.2$. We have thus made an experimental quantification of the magnitude of the drag coefficients for *C. elegans* swimming in a fluid.

The second fitting parameter allows for a small horizontal time shift in the data. A phase shift is to be expected for several reasons, including damping of the force transducer, inertial effects of the worm, and imaging artifacts such as overexposure in the body's direction of travel. The observed phase shifts were always smaller than $T/20$, with $T$ the period of the motion. Deviations between data and theory may be attributed to various sources of error [39].

Although other studies have generated predictions of the forces and powers involved in undulatory microswimming at larger length scales, they are reliant on theoretical models, including RFT [27,28]. The close agreement between the predictions of RFT and our experimental data demonstrates the applicability of this model in generating quantitative predictions in undulatory systems (Fig. 3). For the purposes of comparing our measured drag coefficients with theoretical predictions by Lighthill [10], we can use $1.0 \pm 0.2$ mm as an estimated wavelength, and $45 \pm 5$ $\mu$m as the typical thickness of a young adult. Substituting these parameters into Lighthill's expressions, we get $c_N = 4.9 \pm 0.4$, and $c_T = 3.0 \pm 0.3$, which fall within the error of our experimental values.

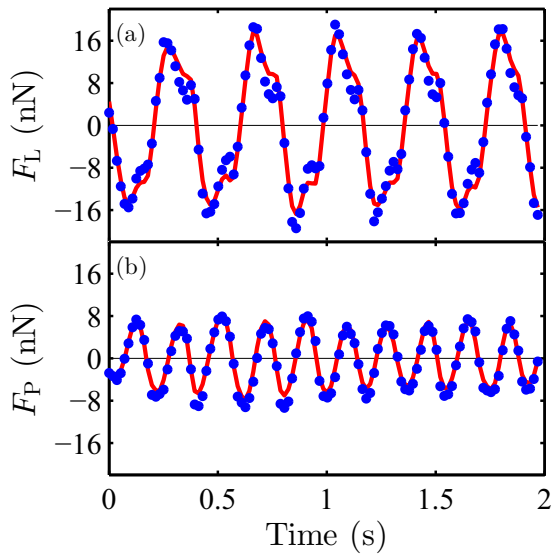


FIG. 3. (Color online) (a) The lateral and (b) propulsive force plotted as a function of time over several periods. The blue circular markers denote the experimental data which contain a systematic error of roughly 10% from uncertainty in the spring constant of the micropipette. The red solid curve represents the prediction from RFT which has been fit to the data. The error in the RFT curve is estimated to be 5%.

Slender body theory (SBT) is a more general model of microswimming, on which the simpler RFT is based [40]. SBT is expected to generate accurate predictions over a wider range of swimming parameters than RFT. However, since RFT captures our data within experimental error, it follows that it is in also in agreement with SBT [39].

Using simple scaling arguments, one can determine the dependence of the magnitudes of typical propulsive and lateral forces upon the worm size. In our experiments, we find that the drag coefficients are largely independent of the size of the worm. Thus, once the forces in Eq. (1) have been integrated over the worm's body, the forces will scale as $F \propto vL_{out}$, where $v$ is a typical speed and $L_{out}$ is the length of the worm outside of the pipette. The typical speed depends on the product of the amplitude ($A$) of the oscillations and the frequency ($f$) of the swimming. Therefore, the forces will scale as $F \propto AfL_{out}$. We make the approximation that the swimming of the worm is self-similar for all life stages, which implies that $A$ will scale linearly with $L_{out}$. This assumption is influenced by previous measurements which showed that mechanical properties of the

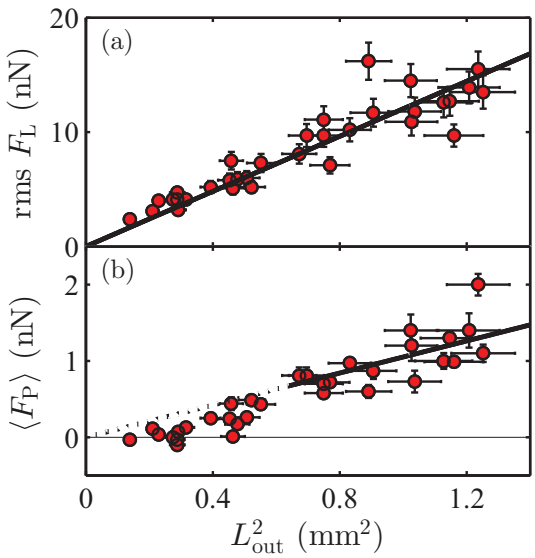


FIG. 4. (Color online) (a) The root-mean-squared lateral force and (b) the mean propulsive force as a function of the square worm length outside of the pipette. The mean and rms are taken over many cycles.

worms can be treated as self-similar [38]. In our experiments, we find that $f$ does not depend on the worm size. Thus, we see that the typical viscous forces generated should scale as $F \propto L^2_{out}$. A plot of the root-mean-squared (rms) lateral force as a function of $L^2_{out}$ yields approximately a straight line passing through the origin, in accordance with the scaling argument [Fig. 4(a)]. Since the worms are attempting to swim forward, one would expect there to be no net force in the lateral direction over one period. Indeed, for the worms, we measure a mean lateral force of $0.1 \pm 0.7$ nN. Consistent with the scaling argument we find that the mean propulsive force $\langle F_P \rangle$ also scales with $L^2_{out}$ at large worm lengths [Fig. 4(b)]. However, at small worm lengths ($\lesssim$800 $\mu$m), the mean force drops. We attribute this to the fact that small worms undergo motions that are quite different from traveling waves and more "hooklike." This type of motion does not yield appreciable propulsion. The mean propulsive forces of larger worms we measure here are comparable to other estimates for *C. elegans* [28].

Here we report a direct measurement of the forces experienced by an undulatory microswimmer. Using micropipette deflection, we attain a high-resolution time sequence of drag forces felt by *C. elegans* while swimming in a buffer. By using these force measurements in conjunction with the low Reynolds number model resistive force theory, we demonstrate the success of this simple model in describing the locomotion of slender microswimmers. This direct verification of the theory, which has previously been assumed to apply at this Reynolds number, provides a better understanding of undulatory microswimming at length scales larger than of unicellular organisms. Furthermore, using RFT to describe our data, we extract measured values of drag coefficients for *C. elegans*, a highly studied model organism and microswimmer. These coefficients are in congruence with theoretical values, and will allow future studies to perform direct calculations of the forces generated by free swimmers simply by using high-speed imaging. Finally, simple scaling arguments successfully explain how the magnitude of lateral and propulsive forces scale with the size of the swimmer.

The financial support by Natural Science and Engineering Research Council of Canada is gratefully acknowledged.

[1] N. Darnton, L. Turner, K. Breuer, and H. Berg, Biophys. J. **86**, 1863 (2004).
[2] D. Weibel, P. Garstecki, D. Ryan, W. Diluzio, M. Mayer, J. Seto, and G. Whitesides, Proc. Natl. Acad. Sci. USA **102**, 11963 (2005).
[3] M. Kim and K. Breuer, Phys. Fluids **16**, L78 (2004).
[4] M. J. Kim and K. S. Breuer, Anal. Chem. **79**, 955 (2007).
[5] Y. W. Kim and R. R. Netz, Phys. Rev. Lett. **96**, 158101 (2006).
[6] M. J. Kim and K. S. Breuer, Small **4**, 111 (2008).
[7] E. Lauga and T. R. Powers, Rep. Prog. Phys. **72**, 096601 (2009).
[8] E. Purcell, Am. J. Phys. **45**, 3 (1977).
[9] M. Silverman and M. Simon, Nature (London) **249**, 73 (1974).
[10] J. Lighthill, SIAM Rev. **18**, 161 (1976).
[11] U. Ruffer and W. Nultsch, Cell Motil. **5**, 251 (1985).
[12] M. Polin, I. Tuval, K. Drescher, J. P. Gollub, and R. E. Goldstein, Science **325**, 487 (2009).
[13] G. Taylor, Proc. R. Soc. London, Ser. A **209**, 447 (1951).
[14] J. Gray, Q. J. Microsc. Sci. **94**, 551 (1953).
[15] J. Gray and G. Hancock, J. Exp. Biol. **32**, 802 (1955).
[16] J. Gray and H. W. Lissmann, J. Exp. Biol. **41**, 135 (1964).
[17] G. Tokic and D. K. P. Yue, Proc. R. Soc. B **279**, 3065 (2012).
[18] R. Cox, J. Fluid Mech. **44**, 791 (1970).
[19] R. S. Berman, O. Kenneth, J. Sznitman, and A. M. Leshansky, New J. Phys. **15**, 075022 (2013).
[20] G. Hancock, Proc. R. Soc. London, Ser. A **217**, 96 (1953).
[21] B. Friedrich, I. Riedel-Kruse, J. Howard, and F. Jülicher, J. Exp. Biol. **213**, 1226 (2010).
[22] K. Drescher, J. Dunkel, L. H. Cisneros, S. Ganguly, and R. E. Goldstein, Proc. Natl. Acad. Sci. USA **108**, 10940 (2011).
[23] N. C. Darnton, L. Turner, S. Rojevsky, and H. C. Berg, J. Bacteriol. **189**, 1756 (2007).
[24] R. P. McCord, J. N. Yukich, and K. K. Bernd, Cell Motil. Cytoskel. **61**, 137 (2005).
[25] S. Chattopadhyay, R. Moldovan, C. Yeung, and X. Wu, Proc. Natl. Acad. Sci. USA **103**, 13712 (2006).
[26] S. Brenner, Genetics **77**, 71 (1974).
[27] C. Fang-Yen, M. Wyart, J. Xie, R. Kawai, T. Kodger, S. Chen, Q. Wen, and A. D. Samuel, Proc. Natl. Acad. Sci. USA **107**, 20323 (2010).
[28] J. Sznitman, X. Shen, R. Sznitman, and P. E. Arratia, Phys. Fluids **22**, 121901 (2010).
[29] X. N. Shen and P. E. Arratia, Phys. Rev. Lett. **106**, 208101 (2011).
[30] X. N. Shen, J. Sznitman, P. Krajacic, T. Lamitina, and P. E. Arratia, Biophys. J. **102**, 2772 (2012).

[31] S. Park, H. Hwang, S.-W. Nam, F. Martinez, R. H. Austin, and W. S. Ryu, PLoS One **3**, e2550 (2008).

[32] T. Majmudar, E. E. Keaveny, J. Zhang, and M. J. Shelley, J. R. Soc. Interface **9**, 1809 (2012).

[33] G. Juarez, K. Lu, J. Sznitman, and P. Arratia, Europhys. Lett. **92**, 44002 (2010).

[34] S. Jung, Phys. Fluids **22**, 031903 (2010).

[35] A. Ghanbari, V. Nock, S. Johari, R. Blaikie, X. Chen, and W. Wang, J. Micromech. Microeng. **22**, 095009 (2012).

[36] J. C. Doll, N. Harjee, N. Klejwa, R. Kwon, S. M. Coulthard, B. Petzold, M. B. Goodman, and B. L. Pruitt, Lab Chip **9**, 1449 (2009).

[37] M.-J. Colbert, A. N. Ragen, C. Fradin, and K. Dalnoki-Veress, Eur. Phys. J. E **30**, 117 (2009).

[38] M. Backholm, W. S. Ryu, and K. Dalnoki-Veress, Proc. Natl. Acad. Sci. USA **110**, 4528 (2013).

[39] See Supplemental Material at http://link.aps.org/supplemental/10.1103/PhysRevE.89.050701 for experimental details, movies of the worm swimming and the forces produced, a calculation of the Reynolds number, and discussion of sources of error and slender body theory.

[40] B. Rodenborn, C.-H. Chen, H. L. Swinney, B. Liu, and H. Zhang, Proc. Natl. Acad. Sci. USA **110**, E338 (2013).